Research Progress on Bandgap and Non-Bandgap Reference Circuits

Guanglong Zhang *

School of Electronic and Information Engineering, Beijing Jiaotong University, Beijing, China

* Corresponding Author Email: 22211317@bjtu.edu.cn u

Abstract. Bandgap reference (BGR) circuits could provide stable, temperature-insensitive reference voltages or currents that are essential to system-level designs. These circuits are extensively employed in critical applications including voltage regulators, oscillators, and analog-to-digital converters (ADCs). Continuous advancements in bandgap reference techniques and CMOS process scaling have significantly enhanced the accuracy and temperature stability of modern reference circuits, making substantial contributions to progress in electronic engineering. This study reviews four classical first-order bandgap reference architectures, with particular emphasis on methods for second-order temperature compensation. Furthermore, it presents a detailed comparison and evaluation of two CMOS-only non-bandgap reference circuit topologies—namely those leveraging the subthreshold characteristics of MOSFETs and those employing capacitor-based biasing techniques. A comprehensive comparative analysis of key performance metrics between bandgap and non-bandgap reference circuits is provided. This research summarizes the architectural differences and performance trade-offs between bandgap and non-bandgap reference circuits, offering valuable perspectives for addressing critical challenges such as stability.

Keywords: Bandgap Reference; Second-Order Temperature Compensation; Non-Bandgap Reference.

1. Introduction

Reference circuits serve as essential modules in mixed-signal integrated circuits which deliver a thermally stable reference voltage or current to the system, thereby establishing a unified reference value for consistent operation. These circuits are extensively utilized in a variety of critical applications, including voltage regulators, and oscillators. In contrast to conventional reference circuits, non-bandgap (CMOS-only) reference architectures offer advantages such as compact area, low power consumption, and structural simplicity. However, they typically suffer from limited accuracy and poor temperature stability.

Recent advancements in analog and mixed-signal IC design have introduced challenges, including stringent power constraints, low-voltage operating ranges for data converters, and noise in reference voltage generation. These issues necessitate highly accurate reference voltage generators to ensure precise system performance.

This paper presents a comprehensive review of reference voltage circuits. Sections 1 and 2 analyze classical bandgap reference architectures and topologies for second-order temperature compensation. Section 3 provides a comparative evaluation of non-bandgap reference circuits, highlighting their strengths and limitations. Finally, Sections 4 and 5 discuss recent research progress in both bandgap and non-bandgap reference circuits.

2. Bandgap Reference Circuit

2.1. Principles of Bandgap Reference Voltage Circuits

Components in electronic circuits often exhibit temperature-dependent characteristics. For instance, the resistance of a resistor varies with temperature—a functional relationship known as the temperature coefficient. Temperature coefficients are generally categorized as positive (PTC) or negative (NTC), and their variation with temperature may involve higher-order functions.

The key to a bandgap reference voltage circuit is using two voltage components with opposing temperature coefficients, which cancel each other to deliver a stable reference voltage.

2.2. Performance Metrics of Bandgap Reference Voltage Circuits

A reference voltage (conventionally denoted as V_{REF}) is delivered by complementary positive and negative temperature coefficient in the reference circuit leverages. Key performance metrics commonly evaluated for such circuits include the reference voltage value, operating voltage range, power consumption, temperature coefficient, and accuracy. The effective temperature coefficient (TC) is a widely adopted metric for characterizing reference voltage circuits. It is defined as the ratio of the relative change in the output quantity to the temperature change across a specified operating range. For reference voltage circuits, the output quantity corresponds to the reference voltage (V_{REF}).

The temperature coefficient is commonly normalized with respect to its value at 25°C(V_{REFnom}). The expression is given as follows:

$$TC = \frac{V_{REFmax} - V_{REFmin}}{V_{REFnom}} \quad (1)$$

2.3. Classical Bandgap Reference Voltage Circuit

The earliest bandgap reference voltage circuit was proposed by American engineer Robert Widlar. A key aspect of the design involves leveraging the complementary temperature characteristics of bipolar devices: the negative temperature dependence inherent in the base-emitter voltage (ΔV_{BE}), combined with the positive temperature dependence exhibited by the difference in base-emitter voltages (ΔV_{BE}) between two transistors biased at different current densities.

By summing these two voltage components, a "zero-temperature-coefficient" reference voltage was achieved. Subsequently, researchers including Kuijk, Brokaw, and Banba further optimized the Widlar architecture, enhancing the performance of circuit. To this day, bandgap reference circuits continue to evolve based on extensions and refinements of this classical bandgap reference framework.

2.3.1. Widlar Circuit

The first bandgap reference voltage architecture was introduced by Widlar [1]. Its architecture is implemented using conventional bipolar circuitry, as illustrated in Figure 1 below.

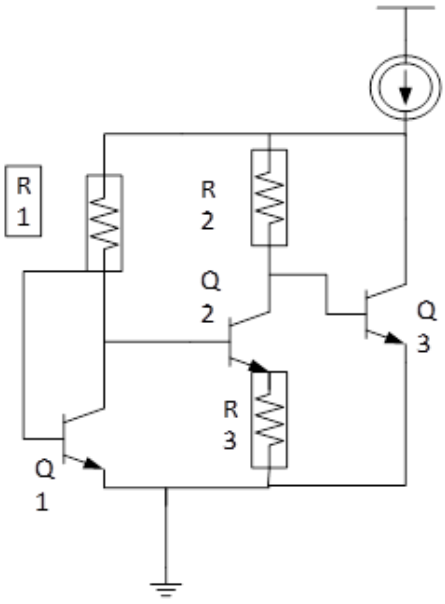

Fig 1. Circuit diagram of the Widlar Bandgap reference.

The reference voltage V_{REF} equals the collector voltage of bipolar transistor Q_3. The voltage difference ΔV_{BE} is derived from the unequal current densities in Q_2 and Q_1, which carry identical currents but differ in emitter junction area.

Transistors Q_1, Q_2, and Q_3 are BJTs of the same type, but Q_2 has an emitter junction area different from those of Q_1 and Q_3. The emitter area of Q_2 is n times that of Q_1. Q_1 and Q_3 are of the same type with equal base-emitter voltages, as $V_{BE1} = V_{BE3}$. The resistances of R1 and R2 are equal. According to Ohm's law, the following relationship holds: $I_{R1} = I_{R2}$.

Given that Q_1 and Q_2 operate at same current and different area, the difference in their base-emitter voltages(ΔV_{BE}) can be satisfied:

$$\Delta V_{BE} = V_{BE1} - V_{BE2} = V_T \ln \frac{I_{C1}}{I_{S1}} - V_T \ln \frac{I_{C2}}{I_{S2}} = V_T \ln n \tag{2}$$

Where V_T denotes the thermal voltage of the BJT, which is proportional to absolute temperature.

Assuming negligible base currents and equal resistances R_2 and R_3. The reference voltage V_{REF} can be satisfied:

$$V_{REF} = V_{BE3} + \frac{R_2}{R_3} \ln n \tag{3}$$

The following equation could ensure temperature independence of the reference voltage:

$$\frac{\partial V_{REF}}{\partial T} = 0 \tag{4}$$

Solving equation (4) under this constraint yields a V_{REF} value of approximately 1.2 V.As indicated by the above equation, the temperature coefficient of V_{REF} in this circuit is mostly determined by resistors R_2 and R_3 and the emitter area ratio of the bipolar transistors. Therefore, satisfying Equation (4) can be achieved by adjusting the emitter area ratio and the resistance values.

However, the Widlar bandgap reference suffers from two main limitations: first, it is challenging to maintain stable collector currents I_{C1} and I_{C2} in the two BJTs; second, the circuit lacks higher-order temperature compensation, resulting in a relatively high temperature coefficient.

2.3.2. Kuijk Circuit and Brokaw Circuit

To mitigate susceptibility to power supply noise in the Widlar reference circuit, Kuijk introduced an operational amplifier into the original architecture [2], as shown in Fig. 2.

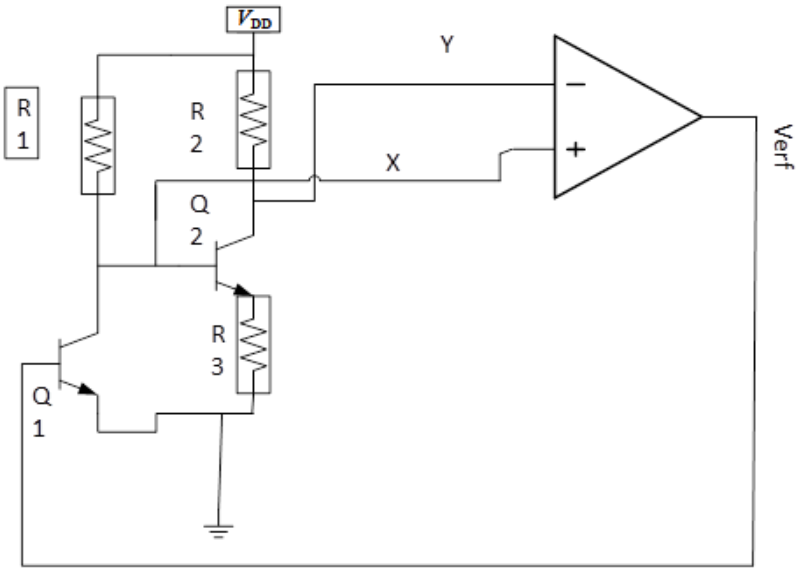

Fig 2. Circuit diagram of the Kuijk bandgap reference.

The added operational amplifier serves two primary purposes: it reduces power supply noise and delivers same voltages of nodes X and Y. By setting resistors R_2 and R_1 to equal values, the currents through them are matched, i.e., $I_{R1} = I_{R2}$.

The emitter area of Q_1 is n times that of Q_2. The current through R_3 is equal to:

$$I_{R3} = V_T \ln \frac{I_{C1}}{I_{S1}} \tag{5}$$

The voltage V_{REF} must be satisfied:

$$V_{REF} = V_{BE1} + \frac{R_2}{R_3} \ln n \tag{6}$$

Compared to the Widlar reference, the Kuijk configuration offers improved performance by eliminating the influence of collector current variations and reducing power supply-induced interference through the use of an operational amplifier. The high gain, low power consumption, and enhanced noise immunity of the op-amp contribute to the circuit's broader applicability and superior performance.

Based on the Kuijk circuit architecture, Brokaw proposed a novel configuration in 1974 [3]. A key innovation involves directly connecting the operational amplifier output to the base terminals of both BJTs. In contrast to the Kuijk configuration, this approach enhances feedback linearity and improves supply noise rejection.

2.3.3. Banda Circuit

In contrast to the voltage summation approach used in the three bandgap reference circuits mentioned above, Banba proposed a bandgap reference based on current summation in 1999 [4]. The circuit schematic is shown in Fig. 3.

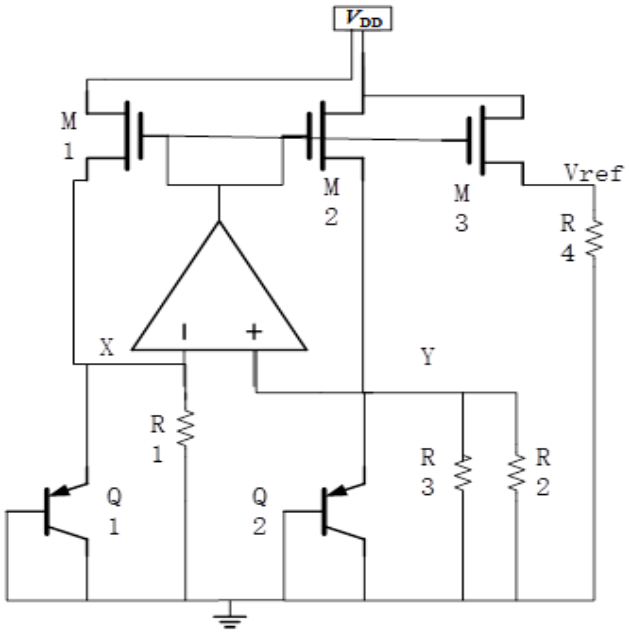

Fig 3. Circuit diagram of the Banba bandgap reference.

This architecture offers greater design flexibility. While the previous two circuits generate a 1.25 V reference voltage, the Banba structure can produce reference voltages below 1.25 V.

A comparative analysis of these classical bandgap reference circuits reveals their distinct characteristics: The Widlar reference suffers from difficulties in stabilizing the collector currents of the two BJTs, high sensitivity to power supply variations, and limited accuracy. The Banba reference operates at low supply voltages with low power consumption and could output reference voltages below 1 V, but its accuracy is compromised by the op-amp's input offset voltage The Kuijk reference incorporates temperature compensation, exhibits low temperature coefficient and power consumption, and offers high power supply rejection ratio (PSRR). Although it also introduces op-amp offset, it demonstrates better process compatibility and broader applicability compared to the Banba structure. The Brokaw reference features low output noise and low quiescent power consumption, but its line regulation performance is relatively poor.

3. Second-Order Temperature Compensation for Bandgap Reference Circuits

In 2005, Avoinne et al. first introduced the concept of second-order compensation, which utilizes a quadratic curvature correction term to mitigate the high-order temperature coefficient of conventional first-order bandgap references, thereby achieving a significantly reduced temperature coefficient [5]. This compensation scheme aims to cancel the higher-order terms in the temperature coefficient. By introducing a compensation voltage term for higher-order nonlinearities into the circuit, the influence of high-order nonlinearities on the output voltage/current is effectively canceled, significantly enhancing the stability and accuracy of the bandgap reference .

3.1. Fundamental Principles of Second-Order Temperature Compensation

Taking the base-emitter voltage (V_{BE}) of a BJT as an example, its value can be expressed by Equation:

$$V_{BE} = V_T \ ln\frac{I_C}{I_S} \tag{7}$$

Where I_S is a higher-order function of temperature T, as given by Equation (11):

$$I_S = b\,T^{4-m}\,exp\left(\frac{-E_g}{kT}\right) \tag{8}$$

Compared to other constant terms, it is evident that V_{BE} exhibits a higher-order dependence on temperature T. Classical bandgap reference circuits address the linear component of the negative temperature coefficient.

Alternatively, V_{BE} can be modeled by Equation (16):

$$V_{BE}\,(T) = V_g(T) - (V_g(T_R) - V_{BE}\,(T_R)\frac{T}{T_R} - (\eta - \delta)V_T\,ln\frac{T}{T_R}) \tag{9}$$

Where T_R denotes the reference temperature, η represents a temperature-dependent coefficient, and δ is a constant associated with the temperature behavior of the current Here, $\eta = 4-\zeta$, with ζ representing the temperature dependence of carrier properties. When $\delta=1$, the current exhibits a negative temperature coefficient; when $\delta=0$, it exhibits a positive temperature coefficient. The term $V_g(T)$ denotes the bandgap voltage at temperature T, expressed in Equation (13):

$$V_g(T) = V_{g0} - bT - c\,T^2 \tag{10}$$

Where V_{g0} , b, and c are characterized over a temperature interval from 150 K to 400 K [6]. Bandgap references using first-order temperature compensation generally exhibit temperature coefficients ranging from 20 to 100 ppm/°C. By comparison, implementations incorporating second-order compensation techniques can achieve significantly lower temperature coefficients, down to 2.9 ppm/°C[7]. Higher-order compensation (third order and beyond) requires more complex circuitry and incurs higher power consumption. Considering the trade-offs between process cost and performance, second-order temperature compensation offers a more balanced solution. Therefore, this paper focuses exclusively on second-order compensation strategies, while higher-order approaches are not discussed.

3.2.Introduction to Second-Order Temperature Compensation Schemes

As indicated by Equation (13), second-order temperature compensation for V_{BE} is required. Advanced compensation circuits that address second and higher-order effects are referred to as curvature correction techniques. Current curvature correction methods primarily include: resistance ratio compensation, piecewise compensation, and precise compensation.

3.2.1. Resistance Ratio Compensation

Resistance ratio compensation is the simplest method for higher-order temperature compensation. It utilizes two resistors with different temperature coefficients (TCs) to achieve the desired compensation [8]. A typical circuit is illustrated in Fig. 4.

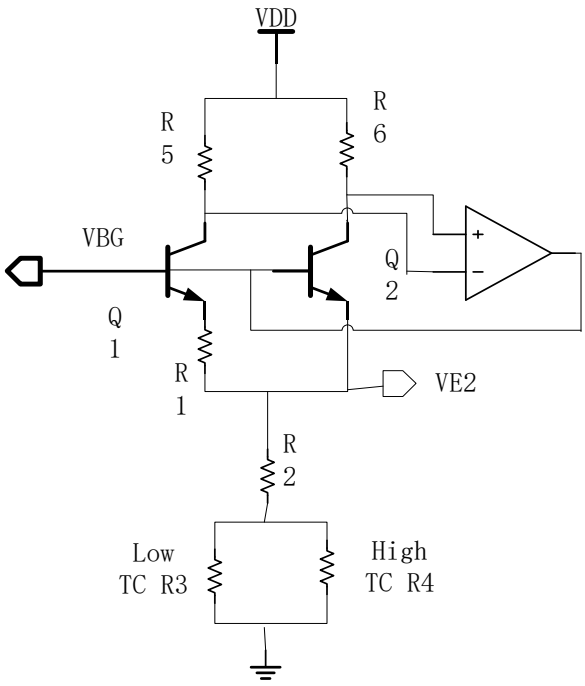

Fig 4. Circuit diagram of the resistance compensation scheme.

Fig. 5 illustrates a circuit incorporating two NPN transistors, denoted as Q_1 and Q_2, with an emitter area ratio of n:1. The circuit includes three thin-film resistors—R_1, R_2, and R_3—exhibiting low temperature coefficients (TC), allowing their temperature dependence to be neglected. Additionally, a diffusion resistor R_4 with a high temperature coefficient is employed. The values of R_5 and R_6 are equal. The operational amplifier forces equal potential at nodes A and B, thereby establishing collector currents in Q_1 and Q_2 that exhibit proportionality to absolute temperature (PTAT). This PTAT current is defined by the following expression:

$$I_{PTAT} = \frac{\Delta V_{BE}}{R_1} = V_T \ ln\, n \tag{11}$$

Where V_T denotes the thermal voltage. The resistance of R_4 equals to $R_{40}(1 + T_C \cdot \Delta T)$, where R_{40} is its nominal value at room temperature, TC denotes the temperature coefficient, and ΔT means the change of temperature.

The equivalent parallel resistance of R_3 and R_4 is given by:

$$R_{3ll4} = \frac{R_{40}\, R_3 \ \ (1 + T_C \cdot \Delta T)}{(1 + T_C \cdot \Delta T) R_{40} \ + R_3} \tag{12}$$

The emitter voltage of Q_2 is equal to:

$$V_{E2} = I_{R_2}\,(R_2 \ + R_{3ll4}) \tag{13}$$

Analysis of Equation (16) indicates that by appropriately selecting the values of R_2, R_3, and R_4, the higher-order terms of V_{BE} can be effectively canceled, achieving low temperature drift characteristics.

Compared to other techniques, this approach only introduces additional resistors to the conventional bandgap reference architecture, resulting in minimal increases in current consumption and layout area. However, it imposes stringent requirements on resistor values and their temperature coefficients.

3.2.2. Piecewise Compensation

The piecewise compensation method involves separate high-temperature and low-temperature compensation circuits. The appropriate compensation circuit is selectively activated due to different operating temperatures. A specific circuit diagram [9] is shown in Fig. 5, which illustrates the use of distinct compensation circuits for high and low temperature intervals, each activated within its respective thermal range.

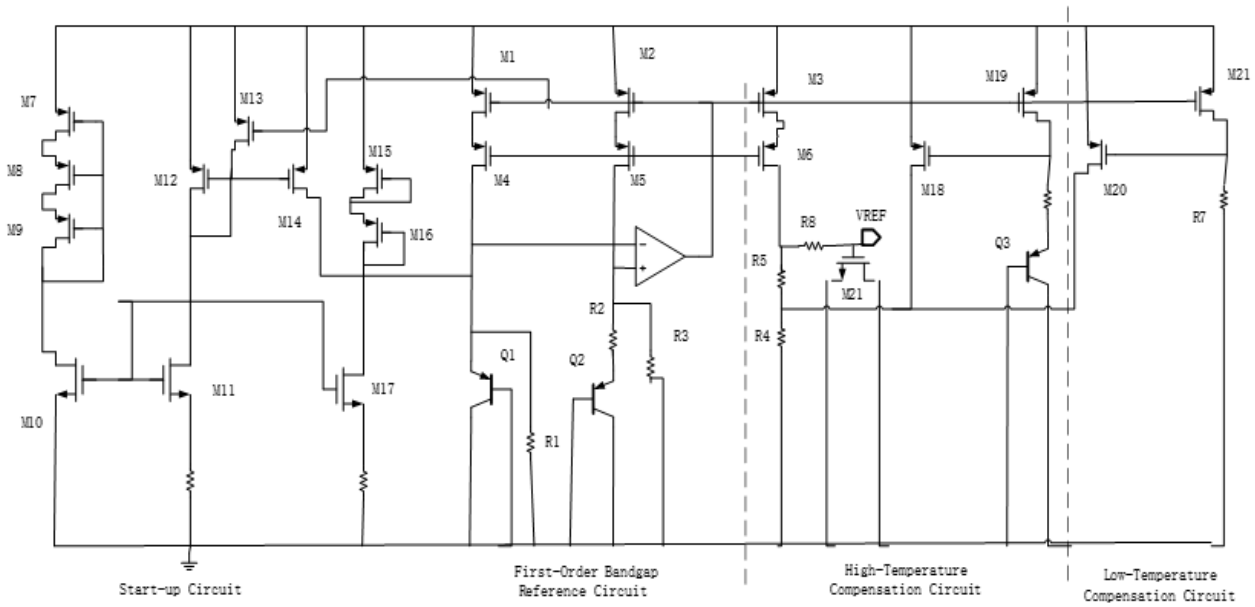

Fig 5. Circuit diagram of the piecewise compensation scheme.

The compensation circuit is divided into high-temperature and low-temperature compensation sections. The high-temperature compensation circuit, operating in the subthreshold region, consists of MOSFETs M_{18}, M_{19}, M_{20}, a negative-temperature-coefficient (NTC) resistor R_6, and a bipolar transistor Q_3. M_{19} mirrors the zero-temperature-coefficient (ZTC) current I_1 flowing through M_1 or M_2. This current passes through R_6 (NTC), generating a negative-temperature-coefficient voltage, which produces a high-temperature compensation current I_{HT} that increases with temperature. The gate voltage V_{G18} of M_{18}, operating in the subthreshold region, is equal to:

$$V_{G18} = I_1 R_6 + V_{BE3} \tag{14}$$

The current I_{HT} is equal to:

$$I_{HT} = I_0 K_{18} exp\left(\frac{V_{GS18} - V_{TH18}}{\eta V_T}\right) \tag{15}$$

Where K_{18} and V_{G18} are known.

The low-temperature compensation circuit, also operating in the subthreshold region, comprises M_{20}, M_{21}, and a positive-temperature-coefficient (PTC) resistor R_7. M_{21} mirrors the ZTC current I_1 from M_1 or M_2. This current flows through R_7 (PTC), producing a positive-temperature-coefficient voltage, which generates a low-temperature compensation current I_{LT} that increases as temperature decreases. The gate voltage V_{G20} of M_{20} is:

$$V_{G20} = I_1 R_7 \tag{16}$$

The current I_{LT} is then given by:

$$I_{LT} = I_0 K_{18}\, exp\left(\frac{V_{GS20} - V_{TH20}}{\eta V_T}\right) \tag{17}$$

The overall reference voltage V_{REF} is expressed as:

$$V_{REF} = \left(\frac{V_{BEQ1}}{R_1} + \frac{V_{BEQ1} - V_{BEQ2}}{R_2}\right)(R_3 + R_4) + (I_{LT} + I_{HT})R_4 \quad (18)$$

In this configuration, M_{17} provides the bias branch for the first-order temperature coefficient, while M_{19} mirrors the ZTC current from M_1 and M_2 to generate a negative-TC voltage across R_6 [8].

The uncompensated reference voltage varies from a maximum of 1.075 V to a minimum of 1.0733 V, with a total variation of 1.7 mV and a temperature coefficient (TC) of 9.85×10^{-6}/°C. After compensation, the reference voltage is nearly 1.075652 V, with a TC of 1.58×10^{-6}/°C, indicating a significant improvement in temperature stability.

3.2.3. Piecewise Compensation

A common approach for precision compensation involves designing compensation circuits based on the current or voltage characteristics of bipolar transistors with different temperature behaviors, building upon a first-order bandgap reference architecture.

To address this, Huang et al. proposed a method utilizing MOSFETs and BJTs to generate a compensating term that deals with the higher-order nonlinear component $T\ln(T)$in the base-emitter voltage [10]. The circuit module for precision compensation is illustrated in Fig 6.

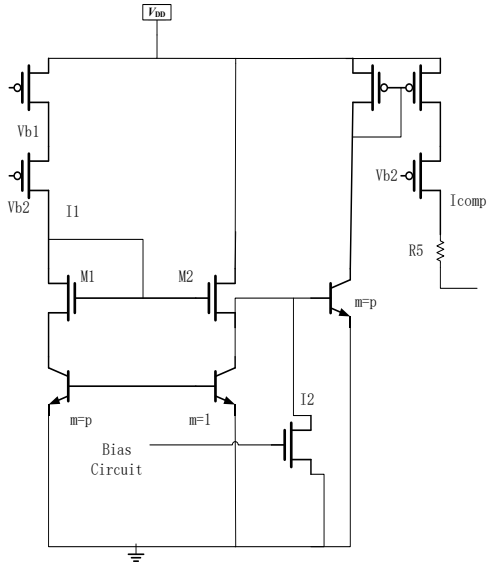

Fig 6. Circuit diagram of the precision compensation scheme.

In Fig 6, I_1 and I_2 are bias currents generated by the operational amplifier and the base-emitter voltage difference of the transistors, respectively. Their values are given by:

$$I_1 = P_1 T \frac{k \ln 2}{q R_8} \quad (19)$$

$$I_2 = P_2 \frac{V_{BE2}}{R_9} \quad (20)$$

Where P_1 and P_2 are mirroring ratio coefficients. The target compensation current I_{comp} is expressed as:

$$I_{comp} = I_1 \exp\left(\frac{\sqrt{\frac{2}{\mu(T)C_{ox}\frac{W_c}{L_c}}}\left(\sqrt{I_1} - \sqrt{\frac{1}{p}I_1 + I_2}\right)}{V_T}\right) \quad (21)$$

This expression indicates that I_{comp} exhibits strong temperature dependence and nonlinearity. The design objective of the higher-order temperature-compensated bandgap voltage reference is to mitigate the $T\ln(T)$ component inherent in V_{BE}. By carefully designing the circuit, I_{comp} can be aligned with the $T\ln(T)$ term, thereby achieving effective compensation. Without introducing I_{comp}, the temperature coefficient (TC) is 9.3 ppm/°C. After applying higher-order compensation, the TC is reduced to 0.611 ppm/°C, demonstrating significant improvement in nonlinear curvature correction.

3.2.4. Other Compensation Schemes

In 1994, Lee et al. first proposed an exponential temperature compensation scheme [11]. This method utilizes the temperature-dependent current gain β of bipolar transistors to generate an exponential compensation voltage that counteracts the higher-order curvature of V_{BE}, thereby enhancing its linearity.

The current gain β exhibits an inverse exponential relationship with the emitter doping concentration, expressed as:

$$\beta(T) = \beta_{\infty}\ exp\left(\frac{-\Delta E_G}{kT}\right) \tag{22}$$

Where $\beta(T)$ means the current gain at temperature T, β_{∞} is the asymptotic current gain, ΔE_G is the Energy bandgap reduction, and k is the Boltzmann constant.

This formulation indicates that as temperature TT increases, the current gain β grows exponentially, thereby compensating for the higher-order curvature of V_{BE}. Experimental results demonstrate that this approach attains a 1.45 ppm/°C temperature coefficient without requiring additional circuitry—only adjustments to transistor dimensions are necessary.

4. Non-Bandgap Reference Circuits

As the name implies, non-bandgap reference circuits do not utilize the bandgap voltage as a reference. Instead, as shown in Fig.7, they can be understood as CMOS-only reference circuits that exclude bipolar junction transistors (BJTs). Compared to bandgap reference circuits, non-bandgap architectures often lack effective temperature compensation mechanisms. A common implementation involves circuits that leverage the threshold voltage (V_{th}) of CMOS transistors as a reference element. Such implementations generally suffer from substantial temperature-induced variation owing to inadequate compensation mechanisms Shown below is a typical CMOS-based non-bandgap reference circuit [12].

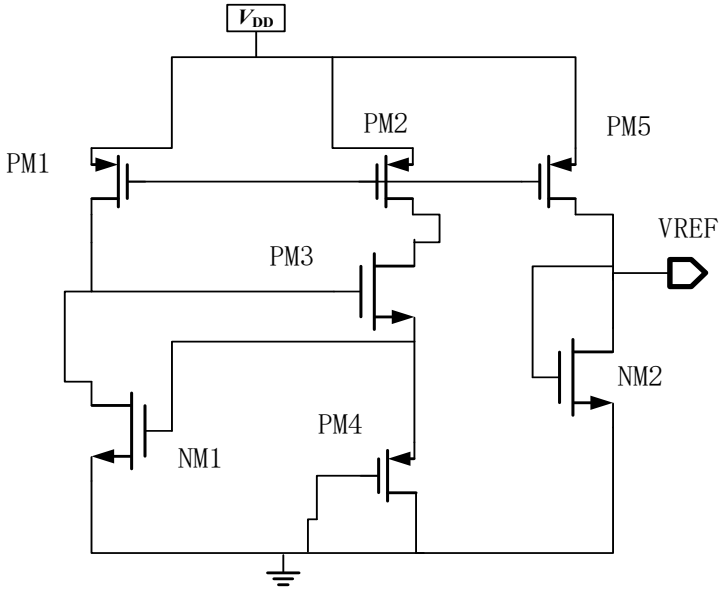

Fig 7. Circuit diagram of the non-bandgap reference.

Circuit analysis reveals that PM_3 and NM_1 function in the subthreshold regime, whereas PM_4 operates in the linear region and may be represented as an equivalent resistor. The current I_{PTAT} is determined as follows. Under subthreshold operation, the gate-source voltage of NM_1 complies with the following expression:

$$V_{GS_{N1}} = V_{TH_{N1}} + mV_T + ln\left(\frac{I_{DS_{N1}}}{{V_T}^2 \mu_{N1} C_{ox} K_{N1}}\right) \tag{23}$$

PM_4 operates in the linear region, and its equivalent resistance can be expressed:

$$R_{on_{P4}} = \frac{1}{\mu_P C_{ox} K_{P4}\left(V_{GS_{N1}} - V_{TH_{P4}}\right)} \tag{24}$$

Let $\mu_P C_{ox} K_{P4} = \beta_{P4}$. Differentiating both sides of Equation (24) with respect to temperature yields:

$$\frac{\partial R_{on_{P4}}}{\partial T} = \frac{\partial V_{TH}}{\partial T} = \frac{1}{{\beta_{P4}}^2 \left(V_{GS_{P4}} - V_{TH_{P4}}\right)^2} \tag{25}$$

From Equation (25), it is evident that since $\frac{\partial V_{TH}}{\partial T}$ is negative, the equivalent resistance has a negative temperature coefficient, meaning its value decreases as temperature increases. Given that the currents in the two branches of the bias circuit are equal, i.e., $I_{DS_{N1}} = I_{DS_{P4}} = I_{PTAT}$, the following holds:

$$V_{GS_{N1}} = I_{DS_{P4}} \cdot R_{on_{P4}} \tag{26}$$

Substituting Equation (24) and $I_{DS_{N1}} = I_{DS_{P4}} = I_{PTAT}$ into Equation (26):

$$I_{PTAT} = \frac{V_{TH_{N1}} + mV_T\, ln\left(\frac{I_{PTAT}}{{V_T}^2 \mu_{N1} C_{ox} K_{N1}}\right)}{R_{on_{P4}}} \tag{27}$$

To produce the reference voltage, the current is replicated into the NM_2 branch via current mirroring. Assuming the aspect ratios of PM_1, PM_2, and PM_5 are $1 : 1 : a$, the current mirror gain is $1 : a$, yielding the current through NM_2 as:

$$I_{DS_{N2}} = aI_{PTAT} \tag{28}$$

Based on the subthreshold I-V characteristics, the gate-source voltage of NM_2, i.e., V_{REF} is equal to:

$$V_{REF} = V_{GS_{N2}} = V_{TH_{N2}} + mV_T\, ln\left(\frac{a\, I_{PTAT}}{{V_T}^2 \mu_{N2} C_{ox} K_{N2}}\right) \tag{29}$$

Let $\mu_{N2} C_{ox} K_{N2} = \beta_{N2}$. Differentiating both sides of Equation (28) with respect to temperature T gives:

$$\frac{\partial V_{REF}}{\partial T} = \frac{\partial V_{TH_{N2}}}{\partial T} + m\frac{k}{q} ln\left(\frac{aI_{PTAT}}{{V_T}^2 \beta_{N2}}\right) + mV_T \cdot \frac{{V_T}^2 \beta_{N2}}{aI_{PTAT}} \cdot \frac{a{V_T}^2 \beta_{N2} \frac{\partial I_{PTAT}}{\partial T} - 2\frac{k}{q} V_T \beta_{N2} I_{PTAT}}{({V_T}^2 \beta_{N2})^2} \tag{30}$$

In the above equations, V_{TH} denotes the threshold voltage; m represents the subthreshold slope factor; k stands for the Boltzmann constant; C_{ox} indicates the gate oxide capacitance; q means the electron charge; $V_T = \frac{kT}{q}$ defines the thermal voltage; μ corresponds to the carrier mobility; and $K_n = (W/L)_n$ gives the MOS aspect ratio.

Satisfying the condition $\frac{\partial V_{REF}}{\partial T} = 0$ in Equation (37) is challenging, indicating that non-bandgap circuits exhibit limited temperature stability. However, their simple structure and fully CMOS-

compatible implementation result in low power consumption, making them suitable for basic reference voltage applications in everyday scenarios.

Additionally, some studies have proposed alternative approaches, such as using capacitive biasing with active body diodes to generate PTAT and CTAT voltages, replacing traditional BJT-based methods to design BJT-free sub-bandgap reference circuits [13]. A specific circuit diagram is shown in Fig. 8.

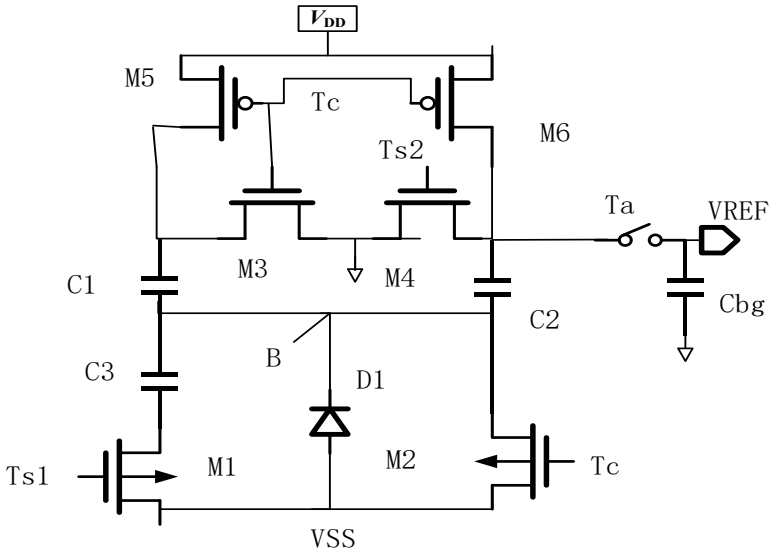

Fig 8. Circuit diagram of the BJT-free sub-bandgap reference.

Leveraging the superior electrical characteristics and strong process compatibility of body diodes, Eberlein et al. proposed a resistor-free sub-bandgap reference circuit in 2020, which replaces traditional BJTs with body diodes and incorporates capacitive biasing. The capacitor is initially charged to a voltage exceeding the diode's built-in potential (>0.8 V) and subsequently discharged through the diode. After a brief transient period, the diode voltage exhibits a logarithmic dependence:

$$V_D(t) \cong \eta \cdot V_T \cdot ln\left(\frac{C \cdot \eta \cdot V_T}{I_S \cdot t}\right) \tag{31}$$

where η is the diode ideality factor, V_T is the thermal voltage (proportional to temperature), I_S is the reverse saturation current, C is the capacitance, and t is the discharge time. Over multiple decades of discharge time, $V_D(t)$ strictly adheres to this logarithmic behavior and is nearly independent of the initial bias condition.

The circuit operates by charging and discharging capacitors C_1 and C_2 to generate a diode voltage $V_D$with CTAT (Complementary to Absolute Temperature) characteristics. Through reverse charge sharing between capacitors, the bandgap reference voltage V_{REF} is derived as:

$$V_{REF} = V_D(t_{s2}) - \frac{C_1}{C_1 + C_3} V_D(t_{s1}) \tag{32}$$

This scheme achieves an output voltage $V_{REF} \approx 370\ mV$, operates within a supply voltage V_{DD} range of 0.85 – 1.05 V, consumes only 18 nW (including switch driving circuitry), and occupies a chip area of 1680 μm^2, demonstrating significant advantages over comparable solutions.

Four historically significant circuits—the Widlar reference, the Banba reference, the series capacitive-biased reference, and the piecewise-compensated reference—are analyzed in this paper. The key performance metrics are summarized in Table 1.

The results indicate that non-bandgap reference circuits, represented by the series capacitive-biased architecture, achieve smaller area and lower power consumption. In contrast, bandgap-based references maintain superior performance in temperature coefficient (TC) tuning and operating temperature range.

Furthermore, with ongoing technological advancements, modern reference circuits continue to evolve toward higher process compatibility and improved accuracy, enabling robust integration into advanced analog and mixed-signal systems.

Table 1. Four circuits compared.

	Widlar[1]	Banba[4]	piecewise-compensated[9]	series capacitive-biased[13]
Power	~1.5A	2.2μA	20.44μA	18nW
ΔV_{REF}(mV)	20	3	0.28	2.7
TC(ppm/°C)	~200	N/A	1.58	~44
Area(mm^2)	N/A	0.1	N/A	0.0016

5. Development Status

With technological advancements, bandgap circuits have witnessed numerous innovations. These include self-calibration techniques for fine-tuning the reference voltage to achieve high-precision output [14], the integration of super source followers to enhance voltage stability, and the adoption of novel processes and materials to improve overall performance. Meanwhile, modern applications impose increasingly stringent requirements on power consumption and stability of bandgap references [15]. Challenges such as inherent random offset in operational amplifiers and current mirror mismatches in CMOS-based bandgap circuits remain to be addressed. In the future, with continued progress in CMOS, BiCMOS, and quantum technologies, the temperature stability and process precision of bandgap reference circuits are expected to advance significantly.

6. Conclusion

Voltage references based on bandgap and non-bandgap principles are critical components in analog circuit design. To facilitate a comprehensive understanding of reference circuits, this paper chronologically reviews the evolution of voltage reference architectures, provides an in-depth analysis of various typical second-order temperature compensation schemes, and highlights both breakthroughs and ongoing challenges in bandgap circuit development. Furthermore, a comparative study of non-bandgap reference circuits (CMOS-only) is presented, evaluating the advantages and disadvantages of BJT-based and BJT-free approaches. It is hoped that this work offers valuable insights into future research in Bandgap reference circuit design.

References

[1] WIDLAR R J. New developments in IC voltage regulators[J]. IEEE Journal of Solid-State Circuits, 1971, 6(1):2-7.

[2] KUIJK K E. A precision reference voltage source[J]. IEEE Journal of Solid-State Circuits, 1973, 8(3):222-226.

[3] BROKAW A P. A simple three-terminal IC bandgap reference[J]. IEEE Journal of Solid-State Circuits, 1974, 9(6):388-393.

[4] BANBA H, SHIGA H, UMEZAWA A, et al. A CMOS bandgap reference circuit with sub-1-V operation[J]. IEEE Journal of Solid-State Circuits, 1999, 34(5):670-674.

[5] AVOINNE C, RASHID T, CHOWDHURY V, et al. Second-order compensated bandgap reference with convex correction[J]. Electronics Letters, 2005, 41(5):276.

[6] Jia S , Ye T , Xiao S.A 2.41 ppm/°C bandgap voltage reference with second-order curvature compensation. Int J Circ Theor Appl.2024;52(11):5539-5553.

[7] S. Huang et al., "A Sub-1 ppm/°C Bandgap Voltage Reference with High-Order Temperature Compensation in 0.18-μm CMOS Process," in IEEE Transactions on Circuits and Systems I: Regular Papers, vol. 69, no. 4, pp. 1408-1416, April 2022

[8] K. Zhao, "Design and Research of Low-Temperature Coefficient Low-Power Bandgap Voltage Reference," M.S. thesis, Nanjing Univ. Posts Telecommun., Nanjing, China, 2023.

[9] Q. Haihong and F. Quanyuan, "A design of segmental curvature compensation low temperature drift bandgap reference circuit," Microelectronics, vol. 55, no. 4, pp. 522-527, Aug. 2025.

[10] Y. Huang, L. Zhu, F. Kong, C. Cheung and L. Najafizadeh, "BiCMOS-Based Compensation: Toward Fully Curvature-Corrected Bandgap Reference Circuits," in IEEE Transactions on Circuits and Systems I: Regular Papers, vol. 65, no. 4, pp. 1210-1223, April 2018

[11] Inyeol Lee, Gyudong Kim and Wonchan Kim, "Exponential Curvature-compensated BiCMOS Bandgap References," in IEEE Journal of Solid-State Circuits, vol. 29, no. 11, pp. 1396-1403, Nov. 1994

[12] Y. Jianhui and Y. Jiang, “Design of a Low Temperature Drift CMOS Bandgap Voltage Reference,” M.S. thesis, Guizhou University, Guiyang, China, 2023.

[13] M. Eberlein and H. Pretl, "Recent Developments in Bandgap References for Nanometer CMOS Technologies," 2020 Austrochip Workshop on Microelectronics (Austrochip), Vienna, Austria, 2020, pp. 42-46.

[14] S. K. Lee, et al., "A 0.6-V 14.92-ppm/°C 200-nW Resistorless Bandgap Reference with Double Curvature Compensation and VTH Variation Autocalibration," *IEEE Transactions on Circuits and Systems II: Express Briefs*, vol. 69, no. 3, pp. 1722-1726, Mar. 2022.

[15] B. Razavi, "The Bandgap Reference [A Circuit for All Seasons]," *IEEE Solid-State Circuits Magazine*, vol. 8, no. 3, pp. 9-12, Summer 2016.